High-Resolution MRI Reflects Myeloarchitecture and Cytoarchitecture of Human Cerebral Cortex

Simon Eickhoff,[1,2] Nathan B. Walters,[3] Axel Schleicher,[2] Jillian Kril,[4] Gary F. Egan,[5] Karl Zilles,[1,2] John D.G. Watson,[3] and Katrin Amunts[1]*

[1]*Institute of Medicine, Research Center Jülich, Jülich, Germany*
[2]*C & O Vogt Institute for Brain Research, Heinrich Heine University, Düsseldorf, Germany*
[3]*Department of Medicine, University of Sydney, Sydney, New South Wales, Australia*
[4]*Center for Education and Research on Ageing, University of Sydney, Sydney, New South Wales, Australia*
[5]*Howard Florey Institute, University of Melbourne, Melbourne, Victoria, Australia*

Abstract: Maps of cytoarchitectonically defined cortical areas have proven to be a valuable tool for anatomic localization of activated brain regions revealed by functional imaging studies. However, architectonic data require observations in a sample of postmortem brains. They can only be used reliably for comparison with functional data as probabilistic maps after spatial normalization to a common reference space. The complete architectonic analysis of an individual living brain has not been achievable to date, because the relationship remains unclear between laminar gray value changes of cerebral cortex in magnetic resonance (MR) images and those of cyto- and myeloarchitectonic histologic sections. We examined intensity profiles through the cortex in five imaging modalities: in vivo T1 and postmortem T2 MRI, one cell body stain, and two myelin stains. After visualizing the dissimilarities in the shapes of these profiles using a canonical analysis, differences between the profiles from the different image modalities were compared quantitatively. Subsequently, the profiles extracted from the in vivo T1-weighted images were estimated from profiles extracted from cyto- and myeloarchitectonic sections using linear combinations. We could verify statistically the mixed nature of the cortical T1 signal obtained in vivo: The MR intensity profiles were significantly more similar to myeloarchitectonic than to cytoarchitectonic profiles, but a weighted sum of both fitted the T1 profiles best. *Hum Brain Mapp 24:206–215, 2005.* © 2004 Wiley-Liss, Inc.

Key words: histology; architecture; structure; magnetic resonance imaging; microstructure

INTRODUCTION

The human cerebral cortex is not homogeneous in structure, but can be subdivided into numerous distinct cortical areas, each separated from its neighbors by a unique set of architectonic features, e.g., cyto-, myelo-, and receptor-architectonics [Zilles et al., 2002]. Cytoarchitectonic mapping [e.g., Brodmann, 1909; von Economo and Koskinas, 1925] defines the borders of a cortical area according to changes in the lamination pattern observed in cell body-stained sections. Myeloarchitectonic mapping [e.g., Elliot Smith, 1907; Flechsig, 1920; Vogt and Vogt, 1919] focuses on local variations in size and density of vertical (radial) and horizontal (tangential) fiber bundles. The pioneers of myeloarchitectonic analysis Baillarger [1840] and Elliot Smith [1907] demonstrated that differences in the myelination pattern of cortical areas could be differentiated even at a very low spatial resolution. Baillarger examined the layered architecture of the cerebral cortex by placing thin slices of freshly cut cortex between two glass slides and observing them using a rear projection light [Baillarger, 1840]. Elliot Smith

Contract grant sponsor: National Institute of Mental Health; Contract grant sponsor: National Institute of Neurological Disorders and Stroke; Contract grant sponsor: National Institute of Biomedical Imaging and Bioengineering; Contract grant sponsor: Deutsche Forschungsgemeinschaft; Contract grant number: KFO-112, Schn 362/13-1; Contract grant sponsor: Volkswagenstiftung; Contract grant sponsor: Australian National Health and Medical Research Council; Contract grant sponsor: Australian Brain Foundation; Contract grant sponsor: Neurosciences Victoria.

*Correspondence to: Dr. Katrin Amunts, Institut für Medizin, Forschungszentrum Jülich GmbH, D-52425 Jülich, Germany.
E-mail: k.amunts@fz-juelich.de

Received for publication 27 January 2004; Accepted 28 June 2004
DOI: 10.1002/hbm.20082
Published online in Wiley InterScience (www.interscience.wiley.com).

defined more than 40 cortical areas by careful examination of fresh postmortem brain sections using the naked eye [Elliot Smith, 1907].

High-resolution magnetic resonance imaging (MRI) of postmortem brains yield a resolution of at least 60 μm [Fatterpekar et al., 2002; Walters et al., 2003]. Moreover, new methods have been developed that allow the analysis of human cortical architecture in vivo using high-resolution MRI to a resolution of approximately 280 μm [Barbier et al., 2002; Clark et al., 1992; Walters et al., 2003]. These studies have demonstrated consistently that MRI of the human cerebral cortex is able to reveal a detailed picture of neocortical lamination patterns despite relatively low signal-to-noise ratio of the images. High-resolution MR imaging thus allows the examination of the living human brain on a similar spatial scale, as was available to Baillarger and Elliot Smith for their postmortem studies. It is therefore capable of revealing sufficient detail to enable architectonic differentiation of cortical areas. For example, in a recent study it was demonstrated that neocortical regions of the occipital lobe differ in their laminar pattern visible in MR images, and that a functionally defined cortical region (V5/MT) coincided with a structurally defined region in the high-resolution MR image [Walters et al., 2003].

The precise relationship between the critical lamination patterns revealed in high-resolution MR in vivo images and the cyto- and myeloarchitectonic pattern as obtained from postmortem brains has been a matter of conjecture. Earlier work comparing lamination patterns visible on in vivo T1-weighted MR images with those observed in myelin-stained sections led to suggestions that these patterns mainly reflect changes in the local myelin density [Barbier et al., 2002; Clark et al., 1992]. Others have argued that laminar differences in cell density also influence intensity variations within the cortical gray matter that are observed on in vivo T2-weighted [Yoshiura et al., 2000] and postmortem intermediate-weighted [Fatterpekar et al., 2002] MR images. The relative contribution of these two factors (cortical cell and myelin density) to the resulting MR images, particularly those obtained in vivo, remains an unsolved question, as a quantitative comparison of in vivo MR images with both cyto- and myeloarchitectonic features has not yet been reported. The aim of this study was, therefore, to analyze the relationship between the laminar patterns observed in MR images and those displayed by cyto- and myeloarchitectonic histologic sections in defined cortical areas of the occipital lobe using different MRI acquisition protocols and histologic staining techniques. In particular, we investigated the extent to which myelo- and cytoarchitecture contribute to the cortical lamination patterns obtained from in vivo high-resolution T1-weighted MR images.

MATERIALS AND METHODS

We analyzed two architectonic regions of the occipital lobe: the striate cortex located within and around the calcarine sulcus (area V1), and the adjacent extrastriate visual cortex (likely area V2). The architecture of these two areas was visualized by five imaging modalities (Fig. 1). The respective cortical lamination patterns were then compared statistically. For each modality, brains of four different subjects were included. The modalities were as follows: (1) in vivo T1-weighted structural MRI (T1); (2) postmortem T2-weighted structural MRI (T2); (3) postmortem brains stained for myelin using the black-gold stain (BG); (4) postmortem brains stained for myelin using the Heidenhain-Wölcke stain (HW); and (5) postmortem brains stained for cell bodies using the Nissl-like silver stain (AG).

Volunteers gave informed consent with Ethics Committee approval from the Howard Florey Institute and the University of Sydney. Postmortem specimens were obtained through the donor programs of the Universities of Düsseldorf and Sydney in accordance with the local Ethics Committees. Subjects and brain donors had no history of neurologic or psychiatric diseases. The postmortem brains showed no signs of atrophy or pathologic architectonic features. Mean ages were 37 years for Modality 1 (three males, one female), 70 years for Modalities 2 and 3 (two males, two females), 68 for Modality 4 (two males, two females) and 69 years for Modality 5 (one male, three females). The brains used for Modalities 2 and 3 were identical, as were three of the brains used for Modalities 4 and 5.

Image Acquisition and Preprocessing

Modality 1

In vivo T1-weighted images were acquired on a 1.5-T scanner (Signa Echospeed, General Electric). For each subject, eight coronally oriented high-resolution surface coil T1-weighted images were acquired, using twin flexible surface coils (field of view [FOV], 10 cm) placed over the temporal-occipital region. Aliasing artifacts (superimposed ghost images of slices from the opposite end) were avoided by setting a wide sagittal FOV (3-D fast spoil gradient [FSPGR] sequence, 120 slices, slice thickness: 0.5 mm [no gap], FOV: 16 cm^2, matrix: 288 × 288, in-plane resolution: 0.556 × 0.556 mm^2, echo time [TE]: 3.5 ms, repetition time [TR]: 15.9 ms, inversion time: 350 ms, number of excitations [NEX]: 1, flip angle of 25 degrees). An additional T1-weighted image was similarly acquired by using a volume coil, except with twice the slice thickness, and was used for grayscale normalization. Raw images were transferred via a DICOM client program (Digital Jacket, Hewlett–Packard), composed into contiguous volumes, and saved in Analyze format (Biomedical Imaging Resource, Mayo Foundation, Rochester, MN). Images were segmented manually to remove nonbrain tissue by using MEDx v3.4.1 (Sensor Systems, Sterling, VA). Surface coil signal attenuation was corrected by grayscale normalization [Zhang et al., 2001]. Optimal normalization was achieved with a priori maps of gray matter, white matter, and cerebrospinal fluid (CSF) generated from the volume coil T1-weighted image, applying a nonlinear noise reduction algorithm [Smith and Brady, 1997]. Normalization maps were estimated for each surface coil image and used to generate a series of grayscale-

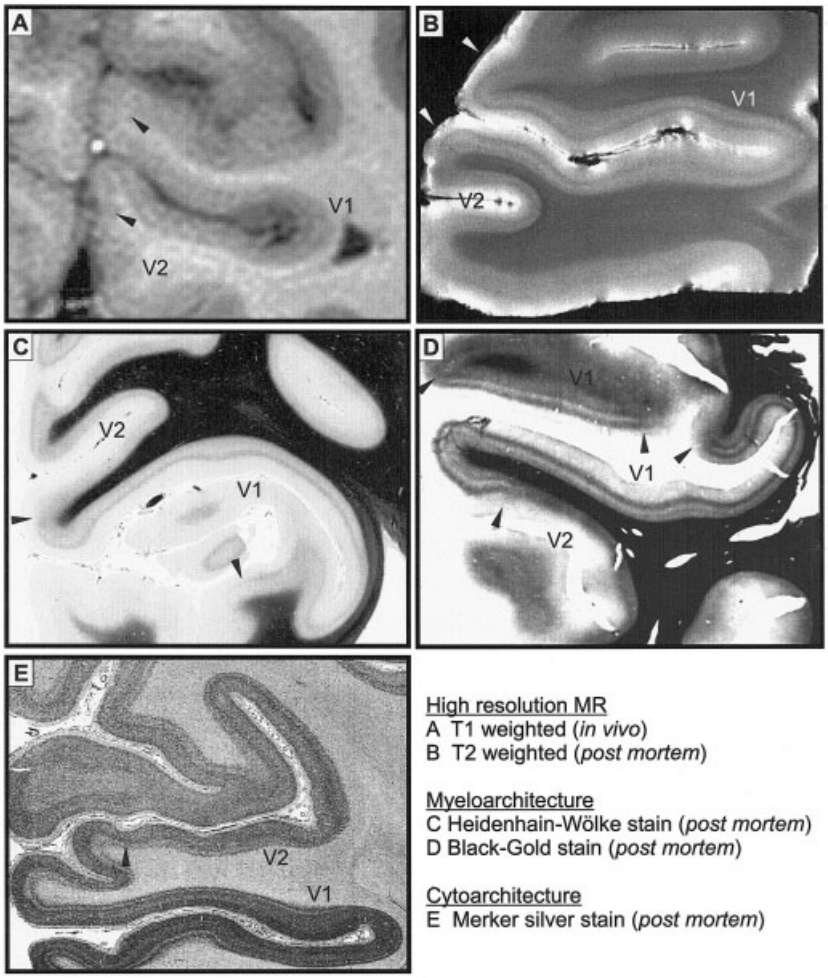

Figure 1.
The striate cortex (V1) and the immediately adjacent extrastriate cortex (likely V2) as displayed by the different modalities. **A:** T1-weighted MRI of a living volunteer [Walters et al., 2003]. **B:** T2-weighted MRI of a postmortem brain [Walters et al., 2003]. **C:** Heidenhain-Wölcke (HW) myelin stain [Romeis, 1989]. **D:** Black-gold (BG) myelin stain [Schmued and Slikker, 1999]. **E:** Silver (AG) cell body staining [Merker, 1983]. The spatial resolution differs between imaging modalities, and ranges from 280 × 280 μm (T1-weighted MRI) to 25 × 25 μm (HW, BG, and AG).

normalized surface coil (GS-SC) T1-weighted images. The eight GS-SC T1-weighted images were realigned using a linear registration tool [Jenkinson and Smith, 2001] resampled at half the acquired voxel dimensions, and averaged by using a softmean function to create a single, high-resolution average [Holmes et al., 1998] T1-weighted image (in-plane resolution: 0.28 × 0.28 mm, slice thickness: 0.25 mm).

Modalities 2 and 3

The postmortem T2-weighted images were acquired at high resolution in a transverse orientation in a Bruker BIOSPEC 47/30 scanner, a horizontal 4.7-T magnet with 30-cm bore. Multislice images were acquired of the histologic specimen after formalin fixation for 2 weeks (number of slices: 12–24, slice thickness: 0.6 mm [no gap], FOV: 30 × 35 mm^2, matrix: 512 × 512, in-plane resolution: 59 × 68 μm^2, TE: 66 ms, TR: 4 s, NEX: 4, acquisition time: 69 min). Specimens were cryoprotected and then serially sectioned at 50 μm in a freezing microtome. After mounting on glass slides, sections were washed, heated, and stained using the black-gold technique [Schmued and Slikker, 1999] until fine fibers of the molecular layer appeared before dehydrating in alcohols, clearing, and coverslipping.

Modalities 4 and 5

The brains used were obtained at autopsy and fixed either in 4% buffered formalin (pH 7.4) or Bodian's fixative (90 ml of 80% ethanol, 5 ml of 37% formaldehyde diluted in water, and 5 ml of glacial acetic acid) for 5 months. The whole paraffin-embedded brains were serially sectioned in the coronal plane (20 μm section thickness) with a microtome for large sections. Series of sections were mounted on glass slides and either silver stained for cell bodies [Merker, 1983] or stained for myelin using the Heidenhain-Wölcke stain [Romeis, 1989]. All histologic staining (black-gold, Heidenhain-Wölcke, and Merker silver stain) was carried out according to standard protocols [Merker, 1983; Romeis, 1989; Schmued and Slikker, 1999].

The histologic sections (Modalities 2–5) were digitized on a flat-bed scanner (AGFA DuoScan f40, Germany) with 25 × 25 μm^2 spatial resolution and 8-bit gray level resolution.

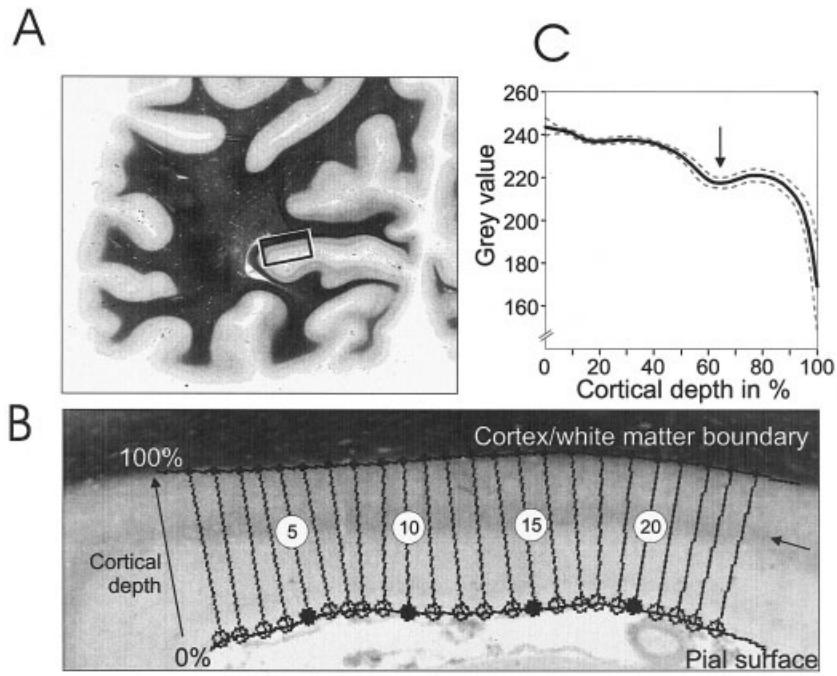

Figure 2.
Extraction of intensity profiles. **A:** Coronal section (left hemisphere) of a human brain stained for myelin (HW). The location of the region of interest (ROI) is marked by a black rectangle. **B:** Higher magnification of same ROI, with superimposed profile lines covering the cerebral cortex from the pial surface to the white matter. Note intense staining for myelin in sublayer IVb (arrow). **C:** Mean gray values profile (dashed lines represent SD). Gray values were not converted into optical densities, but reflect measured data. Profile shows a pronounced dip (arrow) at approximately 60% cortical depth, reflecting the dark staining of the densely myelinated sublayer IVb.

Line Profile Extraction

The cortical lamination patterns of the acquired images for all modalities were quantified by intensity profiles through the cerebral cortex, representing the laminar signal changes from the pial surface to the gray/white matter border. Striate cortex (V1) and immediately adjacent cortex (likely V2) were defined based on microstructural criteria and macroscopic descriptions [Amunts et al., 2000]. For each brain and cortical area, 5–15 regions of interest (ROIs) were analyzed. Each ROI comprised 20–30 profiles (Fig. 2) extending from the pial surface of layer I (outer contour) to the border between layer VI and the white matter (inner contour). The inner and outer contour lines were interactively defined in each image using an image analysis software package (KS 400 v3.0; Zeiss, Germany). The equidistant intensity profiles covering the cortical ribbon of the ROIs were automatically extracted perpendicular to the cortical layers at a spacing of 350 μm using a minimum distance algorithm [Schleicher et al., 2000]. They were subsequently length-normalized to compensate for variations in cortical thickness. Gray values extracted from the myelin-stained sections were converted into optical density values by means of calibration standards using a set of seven calibrated glass standards (Zeiss) in the optical density (OD) range from 0.0 to 2.002. Because the contrast of postmortem T2-weighted images was inverse to the image contrast of the other modalities, their profiles were inverted to enable statistical comparison to the other modalities. Finally, all profiles were z-normalized, to account for intermodal differences in the absolute gray values and intensity ranges.

Dissimilarity Visualization Using Shape-Describing Features

The shape of each profile was quantified by extracting a feature vector of 10 elements [Schleicher et al., 2000], based on central moments [Dixon et al., 1988]: mean y (i.e., mean signal), mean x, standard deviation, skewness, and kurtosis, as well as the analogous parameters from the first derivatives. These parameters and their relationship to the cortical lamination pattern (i.e., the intensity profiles) have been discussed in detail previously [see Amunts et al., 1999; Schleicher et al., 1998, 2000; Zilles et al., 2002]. For each brain and cortical area, a mean feature vector was calculated. A canonical variance analysis [Krzanowski, 1988] based on these mean feature vectors was computed. The degree of dissimilarity between profiles of different modalities was visualized by a scatter plot using the first two canonical variables for each mean feature vector as x and y coordinates.

Quantitative Assessment of Intermodal Differences

Whereas canonical analysis of feature vectors was used to visualize the similarity or dissimilarity in the shape of the profiles within and across modalities, the mean (z-normalized) profiles of the individual subjects were used for all quantitative comparisons, because they directly reflect the signal intensity across the cerebral cortex. The degree of dissimilarity between two modalities was quantified by the mean Euclidean distance (ED) between intermodal pairs of mean profiles. A high mean ED between these profiles indicated a high degree of dissimilarity (thus, low similarity)

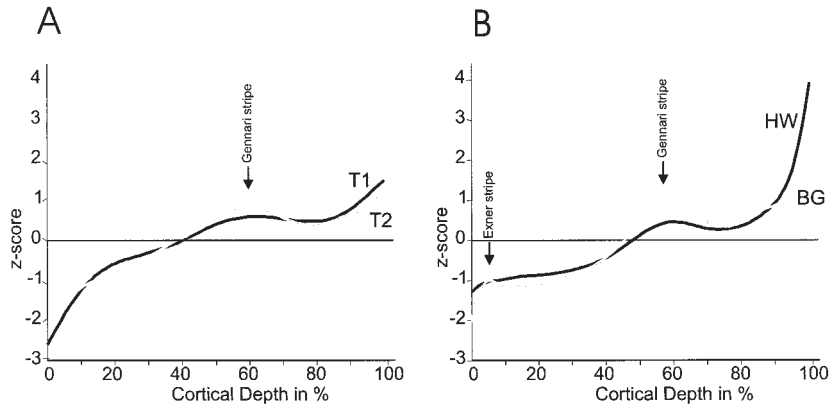

Figure 3.

Average profiles measured in the striate cortex ($n = 4$ subjects). Profiles were z-normalized to enable comparison of profiles with different absolute values. **A:** In vivo T1-weighted MR (black line) vs. postmortem T2-weighted MR (gray line). The T2 profile was inverted for comparison with the T1 profile. **B:** Comparison of profiles from the two myelin stains (HW, black line; BG, gray line). The Gennari stripe (layer IVb) is reflected by a local maximum in the profiles of the HW, BG, T1, and T2 images. The Exner stripe (layer I) is clearly separable only in the profiles obtained in the BG-stained sections.

between the modalities. The calculated differences were then tested statistically using a Student's *t*-test (corrected for multiple comparisons using Bonferroni's method). A significantly lower ED between modalities T1 and HW as compared to the ED between T1 and AG would indicate that profiles of the modality T1 are more similar to those of the HW modality than to profiles of the AG modality.

Estimation of In Vivo Cortical T1 MRI Signal From Histologic Images

The mean in vivo T1 profiles of the striate cortex were estimated by linear combination of mean profiles extracted from myelo- or cytoarchitectonic sections using a least-squares fit. These in vivo T1 profiles were treated as observations whereas profiles from histologic modalities were used as predictors. Each individual mean T1 profile was estimated by all possible pairs of profiles from two predictor modalities. The goodness of fit was quantified by the regression statistic R^2 and (for test purposes) by the ED between the observed profiles and their estimates. To test if a combination of the profiles from two different modalities was significantly more similar to the T1 profiles (i.e., had a significantly lower mean ED) than was the combination of profiles from a single modality, we used the Student's *t*-test. Because four different combinations were tested (HW+BG vs. HW, HW+BG vs. BG, HW+AG vs. HW, and BG+AG vs. BG), *P* values were corrected for multiple comparisons using Bonferroni's method. All calculations were carried out using the MATLAB software package (MathWorks, Natick, MA).

RESULTS

The microstructure of the striate and the immediately adjacent extrastriate cortices were analyzed in five imaging modalities (in vivo T1-weighted MRI [T1], postmortem T2-weighted MRI [T2], Heidenhain-Wölcke myeloarchitecture [HW], Black-Gold myeloarchitecture [BG] and cytoarchitecture [AG]) using intensity profiles through the cerebral cortex.

The group averaged T1 and (inverted) T2 profiles of the striate cortex were highly similar (Fig. 3A). The average laminar patterns of the two myelin modalities (BG and HW) were also very similar, except for a more pronounced peak representing the stripe of Gennari (60% cortical depth) in the BG profile [Vogt and Vogt, 1919] (Fig. 3B). A second, smaller

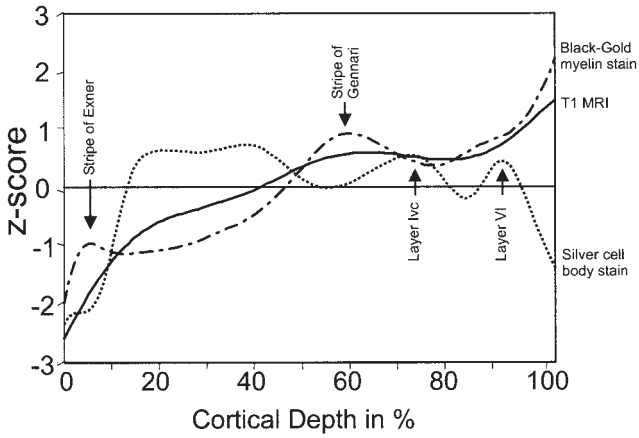

Figure 4.

Group average (four subjects each) profiles of the striate cortex for cyto-, myelo- and MR (T1) architecture. Profiles were extracted from in vivo T1 MR images (solid line), BG myelin (dashed line), and cell body-stained sections (cytoarchitecture, dotted line). Profiles were z-normalized to enable comparison of profiles with different absolute gray values.

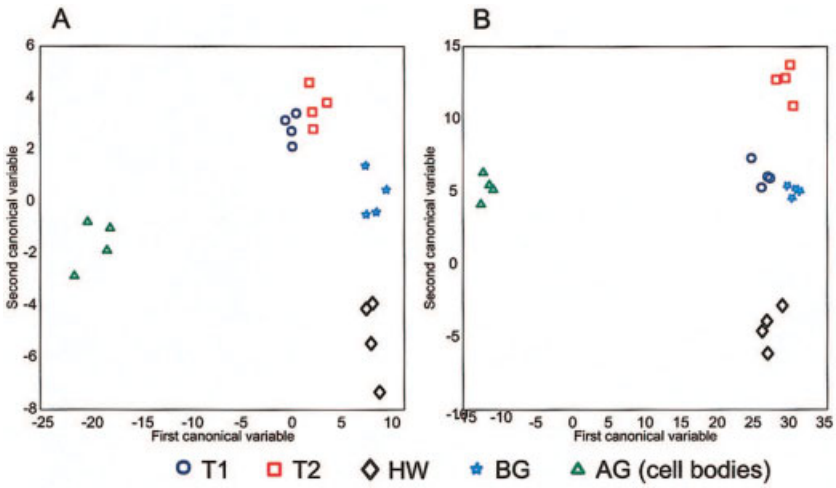

Figure 5.
Canonical analysis of intermodal differences in the shape of the mean profiles extracted from the striate cortex (**A**) and the immediately adjacent extrastriate cortex (**B**). Different symbols represent the relative position of the individual brains in the n-dimensional space. Note the small distance values within one data modality as compared to large distances between clusters, indicating similarity in the shape of profiles from the same image modality and dissimilarity to profiles from another modality.

peak in the BG profile (5% cortical depth) represents the stripe of Exner [Vogt and Vogt, 1919] in layer I.

There was no obvious similarity between the group average MRI and the cytoarchitectonic profiles of the striate cortex (Fig. 4). However, the T1 and the BG myelin profiles showed highly correlated intensity variations in the lower cortical layers. For example, both profiles showed a peak at approximately 60% cortical depth (stripe of Gennari in myeloarchitecture) and a strong signal increase toward the highly myelinated white matter. In the uppermost 10% of the cortex, the intensity of the MR profile was below that of the myelin profile. At between 10–50% cortical depth, this situation was reversed: here, the MRI profile was now higher than the myelin profile. At this cortical depth (10–50%), high intensity values were observed in the cytoarchitectonic profile. The high packing density of cell bodies in the upper cortical layers thus compensates for the difference between the MRI and the myelin profiles. The T1 profile was located between the myelo- and the cytoarchitectonic profiles at more lower cortical depths, further indicating a contribution of both microstructural compartments to the T1 profile.

Modality-specific differences in the shape of profiles extracted from the striate and the immediately adjacent extrastriate cortices were visualized by a canonical analysis based on feature vectors describing the shape of the profiles (Fig. 5). For both areas, all modalities formed distinct clusters, implying a high degree of similarity within a modality and a distinct dissimilarity between the modalities. The two closest (i.e., most similar) clusters of profiles from the striate cortex represented the T1 and the (inverted) T2 profiles, forming a combined "MRI cluster" (Fig. 5A). The two myelin stains (HW and BG) formed a less tightly packed "myelin cluster," with the BG cluster being closer to the MRI profiles. The cytoarchitecture was clearly separated from all other modalities. The analysis of the profiles from the immediately adjacent extrastriate cortex yielded similar results (Fig. 5B): Again, the cytoarchitectonic cluster was most separated. In contrast to the striate cortex, where the T1 and the inverted T2 profiles clustered most closely, the T1 and the BG profiles were most similar in the extrastriate cortex.

Quantification of Intermodal Differences

The mean ED was calculated for inter- and intramodal pairs of profiles from the striate cortex to quantify these observations (Fig. 6, Table I). For all modalities, the intramodal variability (i.e., the differences between profiles from different subjects) was lower than the difference to any other modality, which is in good accordance with the distinct clusters for each modality shown in the scatter-plot, and demonstrates the consistency of the laminar pattern displayed by a given imaging modality across subjects. The lowest intermodal distance was found between the two MR

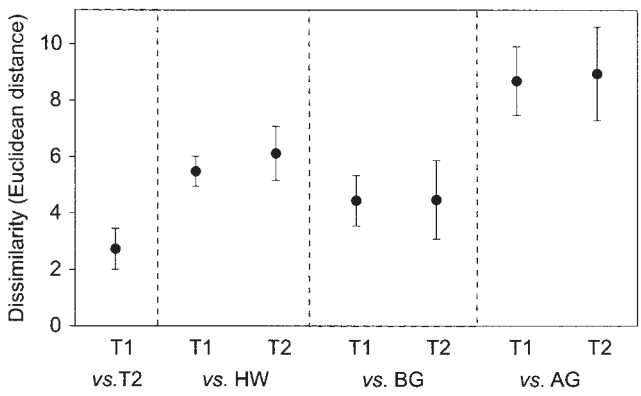

Figure 6.
Mean intermodal Euclidean distances as measures of dissimilarity between profiles from different modalities (error bars represent SD) in the striate cortex. Pairwise comparisons between any two imaging modalities. The two myelin profiles (HW and BG) were significantly more similar (i.e., had smaller distances) to both types of MRI profiles (T1 and inverted T2) than were the AG profiles ($P < 0.05$, corrected for multiple comparisons).

TABLE I. Euclidean distances between individual mean profiles of the striate cortex

	T1	T2	HW	BG	AG
T1	0.94 ± 0.22[a]	2.73 ± 0.72	5.48 ± 0.53	4.44 ± 0.90	8.68 ± 1.21
T2	—	3.37 ± 1.52[a]	6.12 ± 0.96	4.47 ± 1.40	8.94 ± 1.65
HW	—	—	1.47 ± 0.29[a]	4.08 ± 1.44	12.79 ± 1.21
BG	—	—	—	3.66 ± 0.76[a]	11.85 ± 1.10
AG	—	—	—	—	3.47 ± 1.14[a]

Values are given as mean Euclidean distances ± SD. Off-diagonal entries are the Euclidean distances for intermodal pairs, quantifying the degree of dissimilarity between the modalities.
[a] Average Euclidean distances between profiles of the same modality reflect the intramodal variability.
T1, in vivo T1-weighted structural MRI; T2, postmortem T2- weighted structural MRI; HW, postmortem Heidenhain-Wölcke stain; BG, postmortem black-gold stain; AG, postmortem Nissl-like silver stain.

modalities (mean ED between T1 and inverted T2 profiles = 2.73), followed by the distance between the two myeloarchitectonic ones (mean ED between HW and BG = 4.08). Profiles from both myeloarchitectonic modalities were significantly more similar to the in vivo T1 profiles than were the cytoarchitectonic ones (mean ED to the T1 profiles of HW = 5.48, BG = 4.44, AG = 8.68; $P < 0.05$). The comparison of myelo- and cytoarchitectonic profiles with the inverted postmortem T2 profiles confirmed these results: again the myeloarchitecture was significantly more similar to the MRI than was the cytoarchitecture (mean ED to the inverted T2 profiles: HW = 6.12, BG = 4.47, AG = 8.94; $P < 0.05$).

These findings were corroborated by analyzing profiles from the immediately adjacent extrastriate cortex: As for the striate cortex, the MRI profiles were significantly more similar to myelo- than to cytoarchitecture (mean ED to T1 profiles of HW = 4.29, BG = 3.65, AG = 9.65; mean ED to the inverted T2 profiles: HW = 5.22, BG = 3.72, AG = 10.35; $P < 0.05$, Table II).

Estimation of the Histologic Basis of the Cortical T1 Signal

A linear combination of profiles from the two different myelin stains did not result in a significantly better goodness of fit to the T1 profiles than did the pure combination of two individual profiles from either myelin stain alone (combination of HW and BG profiles: ED = 3.775; combination of individual BG profiles: ED = 3.419; combination of individual HW profiles: ED = 4.127; $P > 0.05$ corrected for multiple comparisons; see Fig. 7). However, there was a significant increase in the goodness of fit resulting from the combination of myelo- and cytoarchitectonic profiles (combination of HW and cytoarchitectonic profiles: ED = 2.260; combination of BG and cytoarchitectonic profiles: ED = 2.186; $P < 0.05$).

The value of the regression statistic R^2, indicating the degree to which the combination of different profiles explains the T1 profile, was 0.771 for the combination of individual HW profiles and 0.843 for a combination of individual BG profiles. It increased considerably when myelo- and cytoarchitecture were combined (R^2 of 0.930 for the combination of either HW or BG profiles with cytoarchitectonic ones). In combination, myelo- and cytoarchitecture thus were able to explain 93% of the total variance of the T1 profiles.

The mean weights of the different parameters for the linear estimation of the T1 profiles were: (1) T1 = 0.76 HW + 0.53 AG; and (2) T1 = 0.78 BG + 0.41 AG. The mean weights for the myeloarchitectonic profiles were considerably higher in both cases. This indicates the substantially

TABLE II. Euclidean distances between individual mean profiles of the extrastriate cortex

	T1	T2	HW	BG	AG
T1	1.57 ± 0.60[a]	2.81 ± 0.58	4.29 ± 0.71	3.65 ± 0.75	9.65 ± 0.89
T2	—	2.22 ± 0.40[a]	5.22 ± 0.90	3.72 ± 1.06	10.35 ± 1.18
HW	—	—	1.18 ± 1.18[a]	2.87 ± 0.54	12.93 ± 0.68
BG	—	—	—	2.11 ± 2.11[a]	12.41 ± 0.84
AG	—	—	—	—	2.82 ± 2.82[a]

Values are given as mean Euclidean distances ± SD. Off-diagonal entries are the Euclidean distances for intermodal pairs, quantifying the degree of dissimilarity between the modalities.
[a] Average Euclidean distances between profiles of the same modality reflect the intramodal variability.
T1, in vivo T1-weighted structural MRI; T2, postmortem T2- weighted structural MRI; HW, postmortem Heidenhain-Wölcke stain; BG, postmortem black-gold stain; AG, postmortem Nissl-like silver stain.

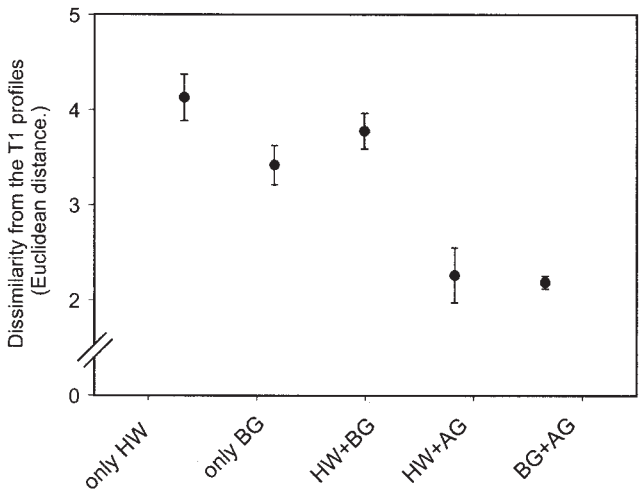

Figure 7.
Mean Euclidean distances between the T1 profiles and their estimates. Profile estimates were linear combinations of HW, BG, and AG profiles as indicated on the *x*-axis. The combination of profiles obtained in myelin-stained sections with profiles obtained in cell body-stained sections (HW+AG and BG+AG) yielded a significantly lower Euclidean distance between the T1 profile and its estimate ($P < 0.05$; corrected for multiple comparisons) than did all other combinations.

higher influence of myelo- over cytoarchitecture on the T1 image.

DISCUSSION

We report the results of a quantitative comparison of the lamination patterns observed in high-resolution MR images of the human cerebral cortex with both myelo- and cytoarchitectonic patterns. This study has shown that the cortical lamination pattern visible on MR images (specifically on those obtained using in vivo T1-weighted MR images) reflects its histologic properties (i.e., myelo- and cytoarchitecture). We used three different, commonly applied histologic staining techniques and two different MR imaging sequences. Only in vivo T1- and postmortem T2-weighted sequences were used to examine the cortical MR architecture, because in vivo T1-weighted imaging has been shown repeatedly to be capable of picking up laminar differences in cortical gray matter. However, T1-weighted images of fixed postmortem brains show only a minimal contrast, even between the gray and white matter [Oros-Peusquens et al., 2003]. In vivo three-dimensional (3-D) T2-weighted images, require extremely long scan times to approach the spatial resolution obtained with the T1 images, and thus are impractical to consider. T2-weighted images are suitable for postmortem imaging because excellent contrast can be obtained between gray and white matter, and scan time is not an issue. Other interesting protocols could have been proton density scans, diffusion tensor imaging, etc., but this was outside the scope of this initial work. The analysis of different, more specifically designed MR sequences and staining methods will certainly further increase and complement our knowledge on the source of the cortical MRI signals.

Visualizing the dissimilarities between the different modalities by canonical analysis (Fig. 5) revealed that profiles extracted from the T1-weighted images and inverted profiles of the T2-weighted images were very similar in shape. Profiles from the two different myelin stains were also highly similar. The lamination pattern revealed by high-resolution MRI was more similar to the myelo- than to the cytoarchitecture.

These observations were statistically confirmed: in both cortical areas, the lowest Euclidean distance (i.e., highest similarity) was observed between the T1 and the inverted T2 profiles. Despite their reverse contrast, both MRI protocols thus reveal similar cortical features, which can be interpreted as MR architecture of the cerebral cortex. In our study, the T2-weighted MR images were acquired from formalin-fixed postmortem brains. Nevertheless, these T2-weighted postmortem MRIs showed a reverse contrast to the in vivo T1 MRI, very similar to in vivo T2 images [Barkhof et al., 1993; Blamire et al., 1999]. In both examined areas very high similarities were also found between the two different myelin stains. This was expected as both methods display, in principal, the same microstructural substrate. The observed distance is supposedly caused by the embedding techniques with differing degrading of myelin or by different biochemical characteristics and thus different specificity of staining techniques [Horton and Hocking, 1997].

All mean EDs between MRI and myeloarchitectonic profiles were significantly lower than were the mean ED between MRI profiles and those from cytoarchitecture. Furthermore, a significant improvement in the goodness of fit of the T1 profile was achieved by combining myelo- and cytoarchitectonic profiles. Although the laminar profiles displayed by the high-resolution T1-weighted MR images therefore depend on both the myelo- and cytoarchitecture of the neocortex, the contribution of these two components to the MR image was not equal but substantially higher for myeloarchitecture than for cytoarchitecture (see formulas 1 and 2). These finding were consistent across subjects, protocols, and cortical areas, allowing more generalized inference about the neuroanatomic substrates of high-resolution MRI. We may conclude that the lamination pattern observed in MR images of the human cerebral cortex originates mainly from its myeloarchitecture with a weaker influence of cell density and cell properties.

This conclusion is in accordance with published observations on the relationship between MR signal intensities and tissue types in the human brain: Clark et al. [1992] and more recently Barbier et al. [2002] observed that a high degree of myelination results in a higher T1 MRI signal. Fatterpekar et al. [2002] proposed a contribution of both myelin and cells to the MR signal. Finally Walters et al. [2003] qualitatively compared exemplary intensity profiles from myelin stains, cell stains, and MR images and argued that the T1 MRI

signal is derived largely from myelin with smaller contributions from cell density.

In contrast and extension to these studies, we have also shown differences in the relationship between MR images and those from histology with respect to the laminar pattern. The most pronounced difference between myeloarchitectonic profiles and the MRI profiles was found in the cell-dense but myelin-sparse upper cortical layers. Yoshiura et al. [2000] observed a depression in the T2 signal for cell-dense regions on in vivo MR images. Due to the reverse contrast between the T2- and the T1-weighted images, this depression of the T2 signal is equivalent to a signal increase in T1-weighted images. This is in good agreement with our own data, where the contribution of the high cell body density in the upper cortical layers compensates for the observed differences between MRI and myeloarchitecture. In a recent study, Lancaster et al. [2003] described a three-pool relaxation model for water-pool fractions in the white matter of in-vivo MR images. Because this model was calculated for white matter, it did not contain a specific intracellular water pool. Based on the T1 relaxation time estimates provided in this study the T1 signal intensity of myelin and the myelinated axons should be expected to be higher than the signals originating from the mixed water pool. This computational model thus explains the high signal intensity observed for the myelin-dense layers in our T1-weighted in vivo images.

CONCLUSIONS

High-resolution structural MRI (T1- as well as T2-weighted scans) displays distinct features of the cortical microstructure when compared to laminar profiles in histologic sections. Although there is a measurable influence of the cytoarchitecture on the intensity of the MRI signal, particularly in the upper cortical layers, the similarity between MR images and myeloarchitectonic sections was much higher in both examined cortical regions. Given this knowledge, cortical regions defined on in vivo MRI can now be related to histologically defined architectonic areas, bridging the gap between in vivo and postmortem studies of the human brain. Conversely cortical areas defined in postmortem studies can be identified in the brains of living volunteers participating in functional imaging studies, or patients being investigated for diagnostic purposes. The precise in vivo identification of cortical areas opens the way for the definition of individual cortical maps. This approach overcomes the problem of large intersubject variability in brain macroscopic and microscopic features [Amunts et al., 1999; Rademacher et al., 1993] when attempting the correlation of structure and function.

ACKNOWLEDGMENTS

We thank Mr. J. Shah for insightful discussions and useful comments on the article. We also thank Ms. U. Blohm, Ms. P. Waley, and Mr. M. Kean for histologic and MRI work, respectively. This Human Brain Project/Neuroinformatics research was supported by grants from the National Institute of Biomedical Imaging and Bioengineering, the National Institute of Mental Health, the National Institute of Neurological Disorders and Stroke (to K.Z. and K.A.), Deutsche Forschungsgemeinschaft (grant KFO-112, Schn 362/13-1 to K.A.), Volkswagenstiftung (to K.Z.), Australian National Health and Medical Research Council (to N.W., G.E., and J.W.), Australian Brain Foundation (to N.W., G.E., and J.W.), and Neurosciences Victoria (to N.W., G.E., and J.W.).

REFERENCES

Amunts K, Malikovic A, Mohlberg H, Schormann T, Zilles K (2000): Brodmann's areas 17 and 18 brought into stereotaxic space—where and how variable? Neuroimage 11:66–84.

Amunts K, Schleicher A, Burgel U, Mohlberg H, Uylings HB, Zilles K (1999): Broca's region revisited: cytoarchitecture and intersubject variability. J Comp Neurol 412:319–341.

Baillarger JP (1840): Mem Acad Med Paris 8:148.

Barbier EL, Marrett S, Danek A, Vortmeyer A, van Gelderen P, Duyn J, Bandettini P, Grafman J, Koretsky AP (2002): Imaging cortical anatomy by high-resolution MR at 3.0 T: detection of the stripe of Gennari in visual area 17. Magn Reson Med 48:735–738.

Barkhof F, Scheltens P, Kamphorst W (1993): Pre-and post-mortem MR imaging of unsuspected multiple sclerosis in a patient with Alzheimer's disease. J Neurol Sci 117:175–178.

Blamire AM, Rowe JG, Styles P, McDonald B (1999): Optimising imaging parameters for post mortem MR imaging of the human brain. Acta Radiol 40:593–597.

Brodmann K (1909): Vergleichende Lokalisationslehre der Großhirnrinde. Leipzig: Barth.

Clark VP, Courchesne E, Grafe M (1992): In vivo myeloarchitectonic analysis of human striate and extrastriate cortex using magnetic resonance imaging. Cereb Cortex 2:417–424.

Dixon WJ, Brown MB, Engelman L, Hill MA, Jennrich RI (1988): BMDP statistical software manual. Berkley: University of California Press.

Elliot Smith G (1907): A new topographical survey of the human cerebral cortex, being an account of the distribution of the anatomically distinct cortical areas and their relationship to the cerebral sulci. J Anat 41:237–254.

Fatterpekar GM, Naidich TP, Delman BN, Aguinaldo JG, Gultekin SH, Sherwood CC, Hof PR, Drayer BP, Fayad ZA (2002): Cytoarchitecture of the human cerebral cortex: MR microscopy of excised specimens at 9.4 Tesla. AJNR Am J Neuroradiol 23:1313–1321.

Flechsig P (1920): Anatomie des menschlichen Gehirns und Rückenmarks auf myelogenetischer Grundlage. Leipzig: Thieme.

Holmes CJ, Hoge R, Collins L, Woods R, Toga AW, Evans AC (1998): Enhancement of MR images using registration for signal averaging. J Comput Assist Tomogr 22:324–333.

Horton JC, Hocking DR (1997): Myelin patterns in V1 and V2 of normal and monocularly enucleated monkeys. Cereb Cortex 7:166–177.

Jenkinson M, Smith S (2001): A global optimisation method for robust affine registration of brain images. Med Image Anal 5:143–156.

Krzanowski WJ (1988): Principles of multivariate analysis. Oxford: Oxford University Press.

Lancaster JL, Andrews T, Hardies LJ, Dodd S, Fox PT (2003): Three-pool model of white matter. J Magn Reson Imaging 17:1–10.

Merker B (1983): Silver staining of cell bodies by means of physical development. J Neurosci Methods 9:235–241.

Oros-Peusquens AM, Shah NJ, Amunts K, Zilles K (2003): Optimised high resolution MRI of the post mortem brain. Presented at the Ninth Annual Meeting of the Organization for Human Brain Mapping, New York, NY. Neuroimage 19(Suppl).

Rademacher J, Caviness VS Jr, Steinmetz H, Galaburda AM (1993): Topographical variation of the human primary cortices: implications for neuroimaging, brain mapping, and neurobiology. Cereb Cortex 3:313–329.

Romeis B (1989): Mikroskopische Technik. München: Urban and Schwarzenberg Verlag.

Schleicher A, Amunts K, Geyer S, Kowalski T, Zilles K (1998): An observer-independent cytoarchitectonic mapping of the human cortex using a stereological approach. Acta Stereol 17:75–82.

Schleicher A, Amunts K, Geyer S, Kowalski T, Schormann T, Palomero-Gallagher N, Zilles K (2000): A stereological approach to human cortical architecture: identification and delineation of cortical areas. J Chem Neuroanat 20:31–47.

Schmued L, Slikker W (1999): Black-gold: a simple, high-resolution histochemical label for normal and pathological myelin in brain tissue sections. Brain Res 837:289–297.

Smith S, Brady J (1997): SUSAN—A new approach to low level image processing. Int J Comp Vis 23:45–78.

Vogt C, Vogt O (1919): Allgemeinere Ergebnisse unserer Hirnforschung. J für Psychologie und Neurologie 25:279–461.

von Economo K, Koskinas G (1925): Die Cytoarchitektonik der Hirnrinde des erwachsenen Menschen. Wien: Springer.

Walters NB, Egan GF, Kril JJ, Kean M, Waley P, Jenkinson M, Watson JD (2003): In vivo identification of human cortical areas using high-resolution MRI: an approach to cerebral structure-function correlation. Proc Natl Acad Sci USA 100: 2981–2986.

Yoshiura T, Higano S, Rubio A, Shrier DA, Kwok WE, Iwanaga S, Numaguchi Y (2000): Heschl and superior temporal gyri: low signal intensity of the cortex on T2-weighted MR images of the normal brain. Radiology 214:217–221.

Zhang Y, Brady M, Smith S (2001): Segmentation of brain MR images through a hidden Markov random field model and the expectation maximization algorithm. IEEE Trans Med Imaging 20:45–57.

Zilles K, Schleicher A, Palomero-Gallagher N, Amunts K (2002): Quantitative analysis of cyto- and receptor architecture of the human brain. In: Mazziotta JC, Toga AW, editors. Brain mapping: the methods. 2nd ed. San Diego: Academic Press. p 573–602.